

# Design of an Experimental Facility for Natural Convection Heat Transfer on an Upper Dome

Suyeon Park<sup>a</sup>, Dong-hyuk Park<sup>a</sup>, Bum-Jin Chung<sup>a\*</sup>

<sup>a</sup> Department of Nuclear Engineering, Kyung Hee University,

1732 Deogyong-daero Giheung-gu Yongin-si Gyeonggi-do, 17104, Republic of Korea

\*Corresponding author: bjchung@khu.ac.kr

**\*Keywords :** Natural convection, Small Modular Reactors, Dome, Truncation angle

## 1. Introduction

The containment vessel (CV) of traditional large nuclear power plants is designed to protect the reactor from missile, contain radioactive materials, and minimize biological effects. However, with the growing interest in Small Modular Reactors (SMR), the size of the reactors and CV has been reduced. Alongside this, there has been an increasing demand for passive safety systems that ensure reactor safety without external power during an accident, adding the function of providing the ultimate cooling mechanism to the containment vessel.

Various pressurized water reactor (PWR) type SMRs are designed to allow the connection between reactor vessel (RV) and CV during an accident, inducing steam condensation. The steam from the RV releases latent heat and condenses as it reaches the cold upper dome of the CV [1-3]. Due to the latent heat, the upper dome of the CV reaches the highest temperature within the CV, making external cooling of the dome crucial for the Passive Containment Cooling System (PCCS).

However, research on external cooling of the dome has not been sufficiently conducted. Additionally, the diameter of licensed or currently designed SMRs, such as Westinghouse at 9.75 m and NuScale's VOYGR at 4.6 m, generally range between 4 to 10 m [4]. Although this is significantly smaller than those of traditional large nuclear power plants, it falls within a very large turbulent range in the scale of natural convection. However, research on the most basic form of a dome, the hemisphere, has been limited to laminar ranges.

Snoek and Tarasuk (1975) conducted heat transfer experiments using an isothermal hemisphere within the laminar range of  $5.36 \times 10^5 \leq Ra_D \leq 6.19 \times 10^5$ , resulting in findings that closely matched McAdams' sphere correlation. Jaluria and Gebhart (1975) also conducted heat transfer experiments using an isothermal hemisphere within the laminar range of  $6.9 \times 10^8 \leq Ra_D \leq 2 \times 10^9$ , observing the formation of a buoyancy plume in laminar flow [5]. Liu et al. (2018) and Swastik Acharya (2022) analyzed the bottom surface effects of the standalone hemisphere structure, also within the laminar range [6, 7]. However, heat transfer research reflecting the structural characteristics of domes in turbulent ranges remains absent. Therefore, this study was planned to observe the changes in fluid flow and heat

transfer in the upper dome at high  $Ra$ , depending on its shape.

## 2. Theoretical background

The characteristics of heat transfer flow in a dome are determined by the truncation angle ( $\theta$ ). The truncation angle is a means of defining the structural characteristics of the dome, determined by cutting a hemisphere in the case of a semi-spherical dome structure. The truncation angle is defined as the central angle from the top point of the hemisphere to the cutting point along the arc, with the center of the hemisphere as the reference point (Fig. 1). The larger the truncation angle, the greater the change in surface slope. The diameter of the dome's base circle is fixed by the diameter of the cylindrical structure ( $D_C$ ), and the truncation angle varies by changing the dome height. A larger truncation angle results in a taller dome, making it closer to a hemisphere, while a smaller truncation angle results in a shorter dome, making it closer to a horizontal plate. In this dome structure, the slope continuously changes from the leading edge to the dome's top point where the slope is zero. As the truncation angle decreases, the maximum slope of the dome also decreases.

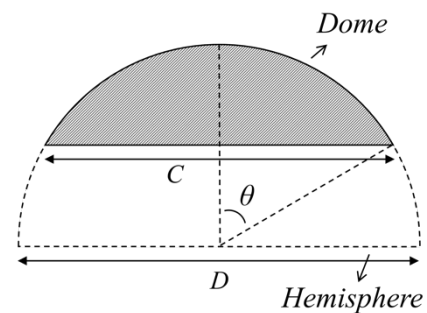


Fig. 1. Truncation angle ( $\theta$ ) concept on dome.

### 2.1 Truncation angle study

Dong et al. (2023) [8] conducted a study using CFD to investigate domes with different truncation angles. The study analyzed the temperature and pressure fields for truncation angles of  $90^\circ$ ,  $75^\circ$ ,  $60^\circ$ ,  $45^\circ$ ,  $30^\circ$ , and  $15^\circ$ . Dong et al. (2023) observed high pressure at the dome top where the plume develops and a low-pressure zone in the middle of the dome surface. They explained that

this pressure gradient influences the flow velocity along the dome surface. The flow along the dome surface reached its maximum velocity at the mid-surface low-pressure zone, then gradually decreased in speed as it moved towards the plume. However, Dong et al. (2023) only studied a limited truncation angle ( $\theta = 45^\circ$ ) and focused on a very low range of  $Ra_w$  ( $w$ : Arc. Length of dome). Since research on the truncation angle of the dome is too limited, such phenomena can be verified through the more extensively studied inclined plate.

### 2.1 Inclined effect on plate

The slope on an upward-facing plate influences the flow differently than expected. Guha et al. (2017) [9] explained that two forces dominate the flow over an inclined plate, with their dominance varying depending on the angle of inclination. Unlike vertical plates, where buoyancy and flow directions are aligned, an inclined plate alters the direction of buoyancy relative to the flow direction, causing a buoyancy force that acts perpendicular to the flow direction to develop. This force generates a pressure gradient perpendicular to the flow direction, making the pressure gradient over the plate no longer negligible. Guha explained that when the inclination angle is small, the flow over the plate is significantly affected by the pressure gradient. Fig. 2 shows the static pressure over an inclined plate analyzed through CFD [10]. The high pressure area corresponds to where the plume develops, and when the inclination angle is less than  $15^\circ$ , the pressure field in the flow direction is non-uniform and variable. This flow influenced by the pressure field was visualized using smoke by Kimura et al. (2002) [11]. Fig. 3 shows the flow patterns over inclined plates at different flow ranges. It reveals that for plates with small inclination angles, the flow is not only upward due to buoyancy but also develops a downward flow along the plate influenced by the pressure field. Kimura named the point where the upward flow from the bottom and the downward flow from the top collide the “collision point” and explained that this point is most influenced by the inclination angle, more so than by factors such as  $Ra$  or the width of the plate. Therefore, this phenomenon can also be observed in dome structures where the surface slope continuously changes.

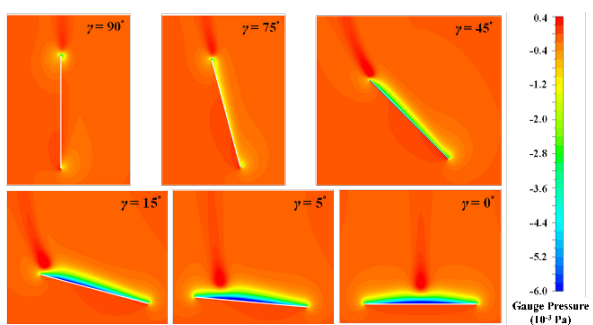


Fig. 2. Pressure contours adjacent to isothermally heated inclined plates at various inclinations of the plate in the range  $0^\circ \leq \gamma \leq 90^\circ$  [Guha et al. (2019)].

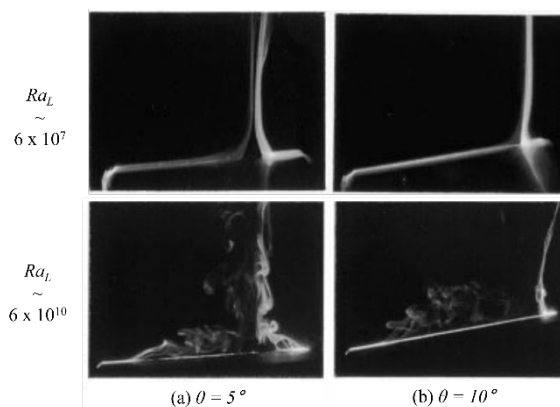


Fig. 3. Flow field with different inclined angle and  $Ra_w$  with observation of collision point [Kiumra et al. (2002)].

## 3. Experimental design

### 3.1 Mass transfer method

In this experiments, heat transfer experiments will be substituted with mass transfer experiments using the analogy concept [12]. The governing equations for heat and mass transfer are analogous and belong to the same mathematical class. In heat transfer system, temperature ( $T$ ) and thermal diffusivity ( $\alpha$ ) can be directly compared to concentration ( $C$ ) and mass diffusivity ( $D_m$ ) in mass transfer systems. In this study, a  $\text{CuSO}_4\text{-H}_2\text{SO}_4$  copper electroplating system was chosen. When an electric potential is applied to electrodes submerged in a  $\text{CuSO}_4\text{-H}_2\text{SO}_4$  aqueous solution and are subsequently reduced at the cathode. The concentration between the cathode surface and the bulk fluid is analogous to the temperature difference between the heater surface and the bulk fluid, while the current density represents the heat flux. However, accurately measuring the concentration of cupric ions at the cathode surface during mass transfer experiments is challenging, so the limit current technique is employed [13]. This experimental technique, based on the heat and mass transfer analogy, has been employed by various researchers [14, 15]. Typically,  $D_m$  is much smaller than  $\alpha$ , making mass transfer systems particularly suitable for simulating fluids with high Prandtl numbers. This system is effective in achieving high  $Ra$ . Table 1 presents the corresponding governing parameters for both heat and mass transfer systems. The mass transfer coefficient ( $h_m$ ) can be obtained by Eq. (1). In this context, the amount of copper ions deposited on the cathode is analogous to the amount of heat transfer. Consequently, the observed electroplating patterns serves as a representation of the local heat transfer patterns [16].

$$h_m = \frac{(1-t_n)I_{lim}}{nFC_b} \quad (1)$$

Table I. Dimensionless numbers for the analogous systems.

Heat transfer		Mass transfer	
$Nu$	$h_b D/k$	$Sh$	$h_m D/D_m$
$Pr$	$\nu/\alpha$	$Sc$	$\nu/D_m$
$Ra$	$g\beta\Delta T C^3/\alpha\nu$	$Ra$	$GC^3/D_m\nu$

### 3.2 Test matrix and rig

Table II shows test matrix. The  $Pr$  was fixed at 2094. Additionally,  $D_C$  and the corresponding  $Ra_{D_C}$  was set to high value of  $1.08 \times 10^{13}$ , ensuring a turbulent flow regime. The truncation angle ( $\theta$ ) of the dome was varied to observe its effect.

Table II. Test matrix

$Pr$	$D_C$ (cm)	$Ra_{D_C}$	$\theta$ (°)
2094	40	$1.08 \times 10^{13}$	90
			30

Fig. 4 shows a schematic of the experimental apparatus along with its electrical circuit diagram. A dome-shaped cathode was placed at the center of an acrylic tank. The cathode was sectioned to observe the variation in heat transfer according to the fluid flow. An anode, measuring 40 cm in length, was positioned at the opposite corners of the acrylic tank to ensure stable electrical current. Power was supplied through a power source (Vüpower K1810), and current was measured and recorded using a DAQ (NI 9227).

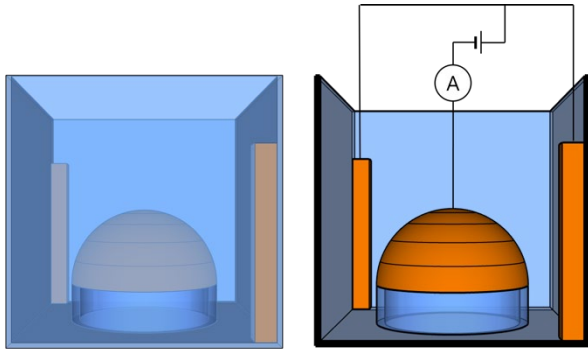


Fig. 4. Overview diagram of the experimental apparatus in upper dome with electrical circuit diagram.

## 4. Conclusions

Through this design, the study aims to analyze the flow characteristics developing the standalone upper dome structure and to examine the impact of the dome's truncation angle on flow development. In particular, for the low truncation angle case, where turbulence begins to develop and pressure is expected to have a significant influence, a different flow patterns is anticipated.

## ACKNOWLEDGEMENT

This work was supported by the Innovative Small Modular Reactor Development Agency grant funded by the Korea Government (MSI) (No. RS-2024-00404240).

## REFERENCES

- [1] E.M.A. Hussein, Emerging small modular nuclear power reactors: A critical review, *Physics Open*, Vol. 5, 2020.
- [2] Z. Liu, J. Fan, Technology readiness assessment of Small Modular Reactor (SMR) designs, *Progress in Nuclear Energy*, Vol. 70, p. 20-28, 2014.
- [3] M. Santinello, M. Ricotti, Long-term decay heat removal in a submerged SMR, *Annals of Nuclear Energy*, Vol. 131, p. 39-50, 2019.
- [4] A. International Atomic Energy, *Advances in Small Modular Reactor Technology Developments A Supplement to: IAEA Advanced Reactors Information System (ARIS) 2020 Edition*, in, International Atomic Energy Agency (IAEA), p. 354, 2020.
- [5] Y. Jaluria, B. Gebhart, On the buoyancy-induced flow arising from a heated hemisphere, *International Journal of Heat and Mass Transfer*, Vol. 18(3), p. 415-431, 1975.
- [6] J. Liu, C.-J. Zhao, H. Liu, W.-Q. Lu, Numerical study of laminar natural convection heat transfer from a hemisphere with adiabatic plane and isothermal hemispherical surface, *International Journal of Thermal Sciences*, Vol. 131, p. 132-143, 2018.
- [7] S. Acharya, Natural Convection Heat Transfer from Upward, Downward, and Sideward Solid/Hollow Hemispheres, *Journal of Thermophysics and Heat Transfer*, Vol. 36(1), p. 141-153, 2022.
- [8] C. Dong, S. Chen, R. Chen, W. Tian, S. Qiu, G.H. Su, Numerical simulation of natural convection around the dome in the passive containment air-cooling system, *Nuclear Engineering and Technology*, Vol. 55(8), p. 2997-3009, 2023.
- [9] A. Guha, K. Pradhan, A unified integral theory of laminar natural convection over surfaces at arbitrary inclination from horizontal to vertical, *International Journal of Thermal Sciences*, Vol. 111, p. 475-490, 2017.
- [10] A. Guha, A. Jain, K. Pradhan, Computation and physical explanation of the thermo-fluid-dynamics of natural convection around heated inclined plates with inclination varying from horizontal to vertical, *International Journal of Heat and Mass Transfer*, Vol. 135, p. 1130-1151, 2019.
- [11] F. Kimura, T. Yoshioka, K. Kitamura, M. Yamaguchi, T. Asami, Fluid flow and heat transfer of natural convection at a slightly inclined, upward-facing, heated plate, *Heat Transfer—Asian Research*, Vol. 31(5), p. 362-375, 2002.
- [12] A. Bejan, *Mass Transfer*, in: *Convection Heat Transfer*, p. 489-536, 2013.
- [13] S.-H. Ko, D.-W. Moon, B.-J. Chung, Applications of electroplating method for heat transfer studies using analogy concept, *Nuclear Engineering and Technology*, Vol. 38, 2006.
- [14] D.W. Hubbard, E.N. Lightfoot, *Correlation of Heat and Mass Transfer Data for High Schmidt and Reynolds Numbers*, *Industrial & Engineering Chemistry Fundamentals*, Vol. 5(3), p. 370-379, 1966.
- [15] F.P. Berger, K.F.F.L. Hau, Mass transfer in turbulent pipe flow measured by the electrochemical method, *International Journal of Heat and Mass Transfer*, Vol. 20(11), p. 1185-1194, 1977.

[16] B.-J. Chung, J.-H. Eoh, J.-H. Heo, Visualization of natural convection heat transfer on horizontal cylinders, *Heat and Mass Transfer*, Vol. 47(11), p. 1445-1452, 2011.